

On priors and scale cuts in EFT-based full-shape analyses

Anton Chudaykin,^{1,*} Mikhail M. Ivanov,^{2,†} and Takahiro Nishimichi^{3,4,5,‡}

¹*Département de Physique Théorique and Center for Astroparticle Physics,
Université de Genève, 24 quai Ernest Ansermet, 1211 Genève 4, Switzerland*

²*Center for Theoretical Physics, Massachusetts Institute of Technology, Cambridge, MA 02139, USA*

³*Department of Astrophysics and Atmospheric Sciences, Faculty of Science,
Kyoto Sangyo University, Motoyama, Kamigamo, Kita-ku, Kyoto 603-8555, Japan*

⁴*Center for Gravitational Physics and Quantum Information,
Yukawa Institute for Theoretical Physics, Kyoto University, Kyoto 606-8502, Japan*

⁵*Kavli Institute for the Physics and Mathematics of the Universe (WPI),
The University of Tokyo Institutes for Advanced Study (UTIAS),
The University of Tokyo, Kashiwa, Chiba 277-8583, Japan*

Parameter estimation from galaxy survey data from the full-shape method depends on scale cuts and priors on EFT parameters. The effects of priors, including the so-called “prior volume” phenomenon have been originally studied in Ivanov et al. (2019) and subsequent works. In this note, we repeat and extend these tests and also apply them to the priors used by D’Amico et al. (2019). We point out that in addition to the “prior volume” effect there is a much more dangerous effect that is largely overlooked: a systematic bias on cosmological parameters due to overoptimistic scale cuts. Unlike the “prior volume” effect, this is a genuine systematic bias due to two-loop corrections that does not vanish with better priors or with larger data volumes. Our study is based on the high fidelity BOSS-like PT Challenge simulation data which offer many advantages over analyses based on synthetic data generated with fitting pipelines. We show that the analysis choices of D’Amico et al. (2019), especially their scale cuts, significantly bias parameter recovery, overestimating σ_8 by over 5% (equivalent to 1σ). The bias on measured EFT parameters is even more significant. In contrast, the analysis choices associated with the CLASS-PT code lead to a negligible ($\lesssim 1\%$) bias in the recovery of cosmological parameters based on their best-fit values.

1. INTRODUCTION

Effective-field theory (EFT) based full shape (FS) analysis is a new tool to extract fundamental cosmological parameters from the shape of the galaxy power spectrum [1–6]. It relies on the EFT of large-scale structure [7–9] and its variants [10–13] for the theoretical modeling of the galaxy clustering data on quasi-linear scales. EFT predictions are approximate as the calculations are carried over only up to a given order of perturbation theory that matches the required precision. EFT models also involve a number of free nuisance parameters which capture the ignorance about the galaxy formation physics on small scales and have to be fitted to data alongside cosmological parameters. EFT-based full-shape results are thus subject to two effects associated with the above lim-

itations.

Any EFT-based full-shape analysis has to assume priors on nuisance parameters in order to ensure that they take physically consistent values. Within the Bayesian framework commonly used in cosmology, the posterior distribution depends on priors by virtue of Bayes’ theorem. Even with informative physically motivated priors, there are residual degeneracies between the EFT and nuisance parameters.¹ For low precision data, some of these degeneracies may result in non-Gaussian posteriors, whose 1D marginalized projections are shifted w.r.t. the best-fit values. This projection effect is often referred to as the “prior volume” effect.² The distance between

* anton.chudaykin@unige.ch

† ivanov99@mit.edu

‡ takahiro.nishimichi@yukawa.kyoto-u.ac.jp

¹ This degeneracy between cosmological and bias parameters is frequentest in nature. This degeneracy exists, for instance, in Fisher forecasts like [14, 15], and affect the parameter estimation even in the absence of any prior volume effects. Reducing this physical degeneracy is the primary goal of the simulation based prior approach of [16–18].

² This nomenclature, strictly speaking, is accurate only when the

the best-fit value and the mean of the 1D marginalized contours does not have any interpretation in the Bayesian framework. Given this reason, “prior volume” effects, especially at the level of $(1 - 2)\sigma$, are not often discussed in the literature.³ In EFT-FS analyses, however, these effects have recently attracted significant attention.

“Prior volume” effects in the context of the EFT-based full-shape analyses were first studied in [1, 5, 22] for the analysis based on the CLASS-PT code [23].⁴ In particular, the full-shape analysis of the BOSS data [25] in [1] estimated them at the 1σ level based on a single chunk of the BOSS data. Refs. [1, 22] pointed out that these effects strongly depend on the volume of the survey, i.e. the quality of data. Results of [1, 22] suggest that they will not represent a problem for the interpretation of results from future galaxy surveys such as Euclid [26] and DESI [27] because the statistical error of these surveys will be smaller than that of BOSS. Even for BOSS the “prior volume” effects can be mitigated in practice in two ways: by including more data (see e.g. [28, 29]), which increases the role of the likelihood, or by using better priors informed from simulations [16–18, 30].⁵

In any realistic analysis “prior volume” effects are coupled with the bias due to two-loop corrections omitted in commonly used one-loop EFT models. Unlike the projection effects, the two-loop corrections represent a genuine theoretical error which does not vanish as the quality of data improves. The theoretical error associated with the two loop corrections has a very steep dependence on the momentum scale cut k_{\max} , e.g. for dark matter in real space it scales as $k^{3.3}$ relative to the linear theory prediction [32, 33]. Thus, a slight increase of k_{\max} from 0.2 hMpc^{-1} to 0.25 hMpc^{-1} increases the error by a factor of 2, and can make it an important source of systematic uncertainty.

A good way to estimate bias due to the theoretical error on estimated cosmological parameters is to fit mock data from numerical simulations. For accurate estimates

one needs to use simulations whose volume is much larger than that of the current surveys. An example is given by the PT Challenge Simulation [34], whose cumulative volume of $566 [h^{-1}\text{Gpc}]^3$ is hundred times larger than the volume of the BOSS survey. The PT Challenge “masked” data were used in the past to validate the scale cuts in EFT-based full-shape analyses. The outstanding fidelity and volume of this simulation allowed one to detect a two-loop systematic error in the BOSS-like data already at $k_{\max} = 0.2 \text{ hMpc}^{-1}$. The method of community challenges that started with the PT Challenge has been recently extended to other methods beyond perturbation theory and beyond the traditional clustering statistics in the Beyond-2pt challenge [35].

The presence of the theory systematic error in EFT-FS analyses shows why parameter projection effects should not be considered in isolation. For instance, one may choose overoptimistic scale cuts or priors in their analysis, which would result in a very small prior volume effect, but both 1D posteriors and the best-fit values will be biased away from the true values. As we show here, this is the case for the analysis choices associated with the PyBird code [36].

Many analyses choices associated with the CLASS-PT code [23] were validated against the PT Challenge simulation in the past. In this note, we repeat and improve these analyses by adjusting them to simulate the BOSS survey as close as possible. This includes the first use of the PT Challenge bispectrum data across the full range of redshifts relevant for BOSS. Previous analyses of refs. [5, 28] were based on the PT Challenge bispectrum at a single redshift $z = 0.61$. In this work we include in the analysis the $z = 0.38$ PT Challenge bispectrum as well. In addition, we study in detail analyses choices associated with the PyBird code, within the same framework.

The use of high-fidelity BOSS-like PT Challenge simulation data offers many advantages over analyses of based on synthetic data generated within the fitting pipeline, done e.g. in [24]. First, it enables the estimation of the theory systematic bias arising from the imperfect modeling of the target statistics. Second, it allows one to estimate the quality of the recovery of true cosmological parameters. Third, the large-volume data allow one to easily estimate the true best-fit model by rescaling the covariance. This method is thus not sensitive to noise in the covariance matrices [14, 37–40] and does not suffer

likelihood has flat directions, so the 1D marginalized posterior is dominated by volume of the prior rather than the likelihood.

³ See e.g. [19–21] for prior volume effects in gravitational wave astronomy.

⁴ The “prior volume” effects in EFT-based full shape analyses were recently revisited e.g. in [24].

⁵ A similar approach was originally put forward in the context of the Halo-Zel’dovich model [31].

from numerical uncertainties associated with the likelihood minimization.

The rest of this note is structured as follows. Section 2 summarizes our main findings. Section 3 compares the analyses choices associated with the CLASS-PT and PyBird codes, while Section 4 presents our main analyses of the PT Challenge simulation data.

2. SUMMARY AND MAIN CONCLUSIONS

We compare analysis choices associated with the PyBird and CLASS-PT EFT-FS likelihoods. Following [34] we dub those two analysis configurations as “West coast” (WC) and “East coast” (EC) models. We also consider two extensions of these models, EC1/2 designed to highlight certain analysis aspects. The EC model that matches the actual BOSS analysis [5] is referred to as EC3. Note that the WC analysis here is the one was used in the actual BOSS analysis [2].⁶

We analyze mock data simulating the BOSS survey. For each model (WC/EC), the datavector is kept the same, while for the covariance we consider two choices: the BOSS covariance extracted from the Patchy mocks [41], and the Gaussian covariance corresponding to a survey with 100 times the BOSS volume across four BOSS data chunks. This choice allows us to get the results free of the parameter projection effects which are equivalent to the best-fit values. Our main results are:

1. WC model tests. The WC analysis choices result in a $0.8\sigma_{\text{BOSS}}$ shift of the posterior mean of ω_{cdm} and introduce a σ_{BOSS} bias in the best-fit value of σ_8 (σ_{BOSS} is the statistical error from the BOSS data). For ω_{cdm} , this is a coupled effect of parameter projection and the inconsistency in the modeling of the stochastic contributions. These two biases can be eliminated by including the scale-dependent stochastic contributions in the monopole and choosing a more conservative k_{max} .

The recovered best-fit value of σ_8 is shifted up by $\approx 5\%$ as a result of the two-loop corrections. This bias remains in the combinations with other datasets like *Planck* CMB. This raises serious concerns on the robustness of results obtained under analyses choices of [2].

This WC case shows that the “prior volume” metric, i.e. the distance between the best-fit and the marginalized mean value, can be misleading if the scale cuts are not calibrated properly. In the WC model the prior volume effect on σ_8 is relatively small, but the best-fit is biased w.r.t. the true value, which impacts parameter recovery.

In addition, the EFT parameter recovery is strongly biased in the WC model. This raises concerns about the robustness of analyses of the non-local primordial non-Gaussianity (PNG), which are sensitive to the EFT bias parameters such as b_2 and $b_{\mathcal{G}_2}$ [16, 42–44].

2. EC model tests. The EC parameter choices lead to the unbiased recovery of h and ω_{cdm} estimated both by best-fits and the 1D marginalized means. The best-fit of the mass fluctuation amplitude σ_8 is recovered with a 1.5% bias, which is negligible given the BOSS error-bars [5, 29]. The peak of the 1D marginalized posterior is shifted down by about 2σ . While this shift somewhat complicates the interpretation of the BOSS-only results, this is entirely a prior effect, which does not affect the ability of the CLASS-PT-based pipeline to recover true cosmological parameters as estimated by their best-fit values. The combinations of BOSS FS-EFT with *Planck* CMB data and other external datasets suppress the prior effects [22, 45]. Hence, our analysis confirms the robustness of the corresponding results obtained with the CLASS-PT based pipeline, e.g. [22, 45–55]. In addition, the prior effects can be mitigated by using more data as in [29], or simulation-based priors [16–18, 30].

3. The validity of the single volume approximation and estimates of parameter projection effects for DESI/Euclid. On the technical side, we present a detailed comparison of our results obtained with the full simulation of the BOSS data across four data chunks with the previous tests based on a single PT Challenge redshift with a covariance rescaled to match the cumulative volume of BOSS DR12 luminous red galaxy (LRG) sample. We call the latter approach a “single volume approximation”.

We find that for WC and early variants of the EC analyses the single volume approximation works reasonably well. For the most recent CLASS-PT based analyses using the galaxy bispectrum [5], however, the single volume approximation underestimates the parameter projection effects. In this case, simulating all sub-volumes of the BOSS data is necessary to accurately access the param-

⁶ It is different from the WC analysis implemented in the PT Challenge [34], which used a more conservative k_{max} value.

eter projection effects. Carrying out this analysis consistently is one of the main results of our study.

Finally, our single-volume results can be treated as an approximation for upcoming surveys such as DESI and Euclid, for which the volumes of individual data chunks will be comparable to the entire volume of BOSS DR12, c.f. [27, 56]. As we show here, in this situation the prior volume effects should not significantly complicate the interpretation of the results from these surveys.

3. COMPARISON OF DIFFERENT ANALYSES CHOICES AND PRIORS

We start off by specifying the relations between different EFT parameters in the WC and EC analysis pipelines.

We start with bias parameters. The WC and EC groups utilize different sets of galaxy bias parameters introduced in [57] and [58]. The WC basis of galaxy biases ($b_1^{WC}, b_2^{WC}, b_3^{WC}, b_4^{WC}$) can be related to the EC basis ($b_1^{EC}, b_2^{EC}, b_{\mathcal{G}_2}^{EC}, b_{\Gamma_3}^{EC}$) as follows

$$\begin{aligned} b_1^{WC} &= b_1^{EC}, & b_2^{WC} &= b_1^{EC} + \frac{7}{2}b_{\mathcal{G}_2}^{EC}, \\ b_3^{WC} &= b_1^{EC} + 15b_{\mathcal{G}_2}^{EC} + 6b_{\Gamma_3}^{EC}, \\ b_4^{WC} &= \frac{1}{2}b_2^{EC} - \frac{7}{2}b_{\mathcal{G}_2}^{EC}. \end{aligned} \quad (1)$$

In what follows we will refer to the linear bias in both models simply as b_1 . We re-express the nonlinear biases in the EC model,

$$\begin{aligned} b_2^{EC} &= -2(b_1 - b_2^{WC} - b_4^{WC}), \\ b_{\mathcal{G}_2}^{EC} &= -\frac{2}{7}(b_1 - b_2^{WC}), \\ b_{\Gamma_3}^{EC} &= \frac{1}{42}(23b_1 - 30b_2^{WC} + 7b_3^{WC}). \end{aligned} \quad (2)$$

The WC model assumes the following priors on bias parameters [2]

$$\begin{aligned} \sqrt{2}(b_2^{WC} + b_4^{WC}) &\sim [-4, 4]_{\text{flat}}, \\ \sqrt{2}(b_2^{WC} - b_4^{WC}) &\sim \mathcal{N}(0, 2^2), \\ b_3^{WC} &\sim \mathcal{N}(0, 2^2). \end{aligned} \quad (3)$$

where $\mathcal{N}(m, \sigma^2)$ is a Gaussian prior centered on m with a standard deviation σ , and the subscript ‘flat’ implies a flat prior with the stated boundaries. These can be

roughly translated into

$$\begin{aligned} b_2^{EC} &\sim [-5.7, 5.7]_{\text{flat}}, \\ b_{\mathcal{G}_2}^{EC} &\in \frac{1}{7} \frac{1}{\sqrt{2}} [\mathcal{N}(0, 2^2) + [-4, 4]_{\text{flat}}] \approx [-0.4, 0.4]_{\text{flat}}, \\ b_{\Gamma_3}^{EC} &\in \approx [-1, 1]_{\text{flat}}. \end{aligned} \quad (4)$$

We approximate these boundaries by gaussian priors, which will be discussed shortly.

We now proceed to the description of the counterterms and stochasticity parameters. The exact relations for those coefficients mildly depend on redshift. In what follows we will focus on the z_3 redshift bin ($z_{\text{eff}} = 0.61$). For the z_1 redshift slice ($z_{\text{eff}} = 0.38$) we found the similar results which we will report in the end of the section. In our calculations we adopt the fiducial Λ CDM cosmology used in the official BOSS analysis [59]: $\Omega_m = 0.31$, $h = 0.676$, $\omega_b = 0.022$, $\sigma_8 = 0.8$ and $n_s = 0.97$. We also adopt $b_1 = 2.2$ from the same BOSS analysis.

The monopole counterterm in different models is specified as follows

$$\begin{aligned} P_0^{\text{ctr.}} \Big|_{\text{EC}} &= -c_0 k^2 \times 2 \cdot \int_0^1 d\mu P_{11}(k) \\ P_0^{\text{ctr.}} \Big|_{\text{WC}} &= c_{ct} \frac{k^2}{k_M^2} \times 2 \cdot \int_0^1 Z_1(\mu) d\mu P_{11}(k), \end{aligned} \quad (5)$$

where [2] assumed $k_M = 0.7 h\text{Mpc}^{-1}$. Matching them, we find the following relation between c_0 and c_{ct} parameters,

$$\frac{c_0}{[\text{Mpc}/h]^2} = -c_{ct} \frac{1}{k_M^2} b_1 \left(1 + \frac{1}{3} \frac{f}{b_1} \right) \approx -5c_{ct} \quad (6)$$

The counterterm for the quadrupole moment reads

$$\begin{aligned} P_2^{\text{ctr.}} \Big|_{\text{EC}} &= -c_2 k^2 \times 2 \cdot 5f \int_0^1 d\mu \mu^2 L_2(\mu) P_{11}(k) \\ P_2^{\text{ctr.}} \Big|_{\text{WC}} &= c_{r,1} \frac{k^2}{k_M^2} \times 2 \cdot 5 \int_0^1 Z_1(\mu) d\mu \mu^2 L_2(\mu) P_{11}(k), \end{aligned} \quad (7)$$

from which we find

$$\frac{c_2}{[\text{Mpc}/h]^2} = -\frac{c_{r,1}}{f} \frac{1}{k_M^2} b_1 \left(1 + \frac{6}{7} \frac{f}{b_1} \right) \approx -7.4 \times c_{r,1}. \quad (8)$$

As far as the stochastic power spectrum is concerned, both models incorporate a constant shot noise contribution and a scale-dependent redshift-space stochastic

counterterm. The latter contributes to the quadrupole moment as follows

$$\begin{aligned} P_2^{\text{stoch.}} \Big|_{\text{EC}} &= a_2 \frac{k^2}{k_{\text{NL}}^2} \frac{2}{3} \frac{1}{\bar{n}_{\text{EC}}} \\ P_2^{\text{stoch.}} \Big|_{\text{WC}} &= c_{\epsilon, \text{quad}} \frac{k^2}{k_M^2} f \frac{1}{\bar{n}_{\text{WC}}} \end{aligned} \quad (9)$$

where $k_{\text{NL}} = 0.45 h \text{Mpc}^{-1}$, \bar{n}_{WC} and \bar{n}_{EC} refer the mean galaxy densities in the WC and EC models. Notice that WC assume $\bar{n}_{\text{WC}}^{-1} = 2500 (h^{-1} \text{Mpc})^3$ and $2200 (h^{-1} \text{Mpc})^3$ for the LOWZ and CMASS redshift bins, whereas in the EC pipeline $\bar{n}_{\text{EC}}^{-1} = 3500 (h^{-1} \text{Mpc})^3$ and $5000 (h^{-1} \text{Mpc})^3$ for z_1 and z_3 slices. Note that the actual measurements from data give $\bar{n}^{-1} = 4800$ and $3500 (h^{-1} \text{Mpc})^3$ for CMASS and LOWZ, respectively [29]. The values of \bar{n} for the z_1/z_3 data split in the EC pipeline correspond to the mean geometric number densities, i.e. the total number of galaxies divided by the effective geometric volume. These numbers are in good agreement with $\bar{n}(z_{\text{eff}})$ measured directly from data using the appropriate weights and selection functions.

Using the above values, for z_3 redshift bin we find the following relation

$$a_2^{z_3} = \frac{3}{2} c_{\epsilon, \text{quad}} f \frac{k_{\text{NL}}^2}{k_M^2} \frac{\bar{n}_{\text{EC}}}{\bar{n}_{\text{WC}}} \approx 0.22 c_{\epsilon, \text{quad}}. \quad (10)$$

For the z_1 chunk we get

$$a_2^{z_1} \approx 0.32 c_{\epsilon, \text{quad}}. \quad (11)$$

Adopting $c_{\epsilon, \text{quad}} \sim \mathcal{N}(0, 2^2)$ from [2], we observe that the WC prior on a_2 is tighter than that in the EC model which is $a_2 \sim \mathcal{N}(0, 1^2)$. The inconsistency of this choice with the physics of the HOD-based galaxies was discussed in [18]. As we will see later, this tight prior reduces the parameter shifts caused by marginalization effects in a multi-chunk full-shape EFT analysis. Importantly, the WC setup also excludes a scale-dependent stochastic counterterm in the monopole, $c_{\epsilon, \text{mono}} = 0$. Although the real-space scale-dependent noise term can be set to zero based on the simulation results [16, 18, 60, 61], the contribution from the $k^2 \mu^2$ counterterm is actually non-negligible, which raises concerns about the choice $c_{\epsilon, \text{mono}} = 0$.

Note that the EC pipeline features the next-to-leading order k^4 redshift-space counterterm \tilde{c} and the real space scale-dependent stochastic noise counterterm a_0 . These

are defined as:

$$P_{\nabla_{\delta}^2}^{\text{ctr}}(k, \mu) = -\tilde{c} k^4 \mu^4 f^4 (b_1 + f \mu^2)^2 P_{11}(k), \quad (12)$$

$$P^{\text{stoch}}(k, \mu) = \frac{1}{\bar{n}} \left(P_{\text{shot}} + a_0 \frac{k^2}{k_S^2} + a_2 \mu^2 \frac{k^2}{k_S^2} \right), \quad (13)$$

with $k_S = 0.45 h \text{Mpc}^{-1}$. The addition of these parameters has minimal impact on the inference of cosmological parameters in the base Λ CDM model. Nonetheless, the EC pipeline incorporates both \tilde{c} and a_0 contributions because it affects the error bars of cosmological parameters. The importance of the $k^4 \mu^4 P_{11}$ counterterm for consistency has been discussed in [1, 18, 23, 33, 62].

To understand what drives the difference in the results between the WC and EC pipelines we perform a series of analyses with different choice of the priors and scale cuts. Below we specify the analysis choices explored in this work.

a. WC model: We adopt the exact priors from the [2, 63], with an analysis of P_0 and P_2 . Below we provide the WC priors on the EFT parameters for each BOSS chunk across the z_1/z_3 redshift bins (if the same prior is applied in both redshifts, we omit the redshift identifier),

$$\begin{aligned} \frac{c_0}{[\text{Mpc}/h]^2} &\sim \mathcal{N}(0, 10^2), \quad \frac{c_2}{[\text{Mpc}/h]^2} \sim \mathcal{N}(0, 60^2), \\ a_2^{z_1} &\sim \mathcal{N}(0, 0.63^2), \quad a_2^{z_3} \sim \mathcal{N}(0, 0.44^2) \\ P_{\text{shot}}^{z_1} &\sim \mathcal{N}(0, 0.11^2), \quad P_{\text{shot}}^{z_3} \sim \mathcal{N}(0, 0.08^2), \\ b_1 &\sim [0, 4]_{\text{flat}}, \quad b_2 \sim \mathcal{N}(0, 5^2), \quad b_{\mathcal{G}_2} \sim \mathcal{N}(0, 0.4^2), \\ b_{\Gamma_3} &\sim \mathcal{N}\left(\frac{23}{42}(b_1 - 1), 1^2\right), \end{aligned} \quad (14)$$

where we approximated the boundaries in eq. (4) by Gaussian priors. Note that the stochastic contributions P_{shot} and a_2 are expressed in terms of the inverse mean galaxy density of the BOSS survey within the EC model.⁷ In total, the WC model has 8 EFT parameters per sky chunk when fitting two multipoles.

Let us now specify the scale cuts in the WC model. The original analyses [2, 63] exploit a slightly different separation into LOWZ ($z_{\text{eff}} = 0.32$) and CMASS ($z_{\text{eff}} = 0.57$) redshift slices, and specify $k_{\text{max}}^{\text{LOWZ}} = 0.2 h \text{Mpc}^{-1}$

⁷ The WC team uses a significantly narrower prior on P_{shot} with a standard deviation of $400 (h^{-1} \text{Mpc})^3$ [2]. Surprisingly, this does not introduce a significant bias in the inference of cosmological parameters in the power-spectrum analyses of the Λ CDM model. The bias could be significant in extensions of this setup.

and $k_{\max}^{\text{CMASS}} = 0.23 h\text{Mpc}^{-1}$, respectively. Since our z_3 slice has effectively a slightly higher redshift and a less data volume than CMASS, we re-scale the original $k_{\max}^{\text{CMASS}} = 0.23 h\text{Mpc}^{-1}$ to $k_{\max}^{z_3} = 0.25 h\text{Mpc}^{-1}$ using Eq. (40) of [2]. We keep $k_{\max}^{z_1} = 0.2 h\text{Mpc}^{-1}$ following [24].

b. EC1 model: We use the WC priors but consistently include a scale-dependent stochastic counterterm in the monopole. Specifically, we add

$$P_0^{\text{stoch.}} \Big|_{\text{EC}} = a_2 \frac{k^2}{k_{\text{NL}}^2} \frac{1}{3} \frac{1}{\bar{n}_{\text{EC}}} \quad (15)$$

where a_2 is taken from (14). In the WC notation, it corresponds to $c_{\epsilon, \text{mono}} \sim \mathcal{N}(0, 1^2)$. The other aspects of the analysis, including the data cuts, remain the same as in the WC model.

c. EC2 model: We adopt the EC priors for the galaxy power spectrum from [5],

$$\begin{aligned} \frac{c_0}{[\text{Mpc}/h]^2} &\sim \mathcal{N}(0, 30^2), \quad \frac{c_2}{[\text{Mpc}/h]^2} \sim \mathcal{N}(30, 30^2), \\ \frac{\tilde{c}}{[\text{Mpc}/h]^4} &\sim \mathcal{N}(0, 500^2), \quad P_{\text{shot}} \sim \mathcal{N}(0, 1^2), \\ a_0 &\sim \mathcal{N}(0, 1^2), \quad a_2 \sim \mathcal{N}(0, 1^2), \\ b_1 &\sim [0, 4]_{\text{flat}}, \quad b_2 \sim \mathcal{N}(0, 1^2), \quad b_{\mathcal{G}_2} \sim \mathcal{N}(0, 1^2), \\ b_{\Gamma_3} &\sim \mathcal{N}\left(\frac{23}{42}(b_1 - 1), 1^2\right), \end{aligned} \quad (16)$$

In total, the EC2 priors consist of 10 parameters. We use the exact same scale cuts and number of multipoles as in the WC and EC1 models.

d. EC3 model: We implement the baseline EC analysis pipeline [5] which additionally includes the power spectrum hexadecapole [22], the real-space power spectrum proxy [64], and the bispectrum monopole [5, 65]. We adopt the EC2 priors for the galaxy power spectrum defined above. We introduce four extra EFT parameters associated with the additional probes, and impose the following priors,

$$\begin{aligned} \frac{c_4}{[\text{Mpc}/h]^2} &\sim \mathcal{N}(0, 30^2), \quad \frac{c_1}{[\text{Mpc}/h]^2} \sim \mathcal{N}(0, 5^2), \\ A_{\text{shot}} &\sim \mathcal{N}(0, 1^2), \quad B_{\text{shot}} \sim \mathcal{N}(0, 1^2). \end{aligned} \quad (17)$$

In total, the EC3 priors consist of 14 parameters.

Following the EC pipeline [5], we change the scale cuts for the galaxy power spectrum to be $k_{\max} = 0.2 h\text{Mpc}^{-1}$ for the z_1/z_3 redshift bins. As we will see later, using a lower value of $k_{\max}^{z_1}$ effectively reduces the systematic bias in parameter recovery. We also adopt $k_{\max} = 0.08 h\text{Mpc}^{-1}$ for the bispectrum measurements.

Note that for any realistic analysis we recommend using the complete analysis pipeline presented in [5], including the full data vector. This corresponds to the EC3 model. The removal of datasets from the total datavector used in [5], e.g. the bispectrum, results in enhanced parameter degeneracies, which increase the bias in parameter recovery.

4. TESTS ON PT CHALLENGE DATA

In this section we test the analysis pipelines using the PT Challenge simulation data. The PT Challenge simulation suite was designed to reproduce clustering properties of the BOSS-like galaxies from the DR12 sample [34]. The total simulation volume is $V = 566 (h^{-1}\text{Gpc})^3$, which is about 100 times larger than the cumulative volume of the galaxy BOSS DR12 sample $V = 5.8 (h^{-1}\text{Gpc})^3$. The large simulation volume provides a stringent test of the theoretical model, allowing us to separate the theory systematic error from the statistical error. This helps assess the origin of parameter shifts and accurately quantify the impact of priors in various analysis setups. We analyze the mean power spectrum and bispectrum over 10 random realizations, for two redshift bins, $z = 0.38$ and $z = 0.61$ that match the effective redshift bins z_1 and z_3 of BOSS DR12. Since the k -binning in the challenge power spectra is quite wide ($\Delta k = 0.01 \text{Mpc}/h$) compared to the fundamental mode of the simulation box, we average our theoretical predictions over each bin as in [5, 34].

We perform two types of analysis. First, we present an analysis of the PT Challenge simulation using the analytical Gaussian covariance.⁸ We adopt the volume and number density specific to the PT Challenge simulation, and adjust the priors accordingly. Second, we carry out a multi-chunk analysis of the four simulation samples using the actual BOSS data covariance estimated from the Patchy mocks. This setup aims to simulate the analysis of the actual BOSS data, allowing us to estimate the impact of priors in the analysis of the real data.

⁸ We neglect the cross-correlation between the power spectrum and bispectrum in the covariance which was shown to be a good approximation for the scales of interest [65].

4.1. PT Challenge analysis

In this analysis we adjust the priors by using the actual value of the mean number density in the PT challenge simulation, $\bar{n}_{\text{PTC}}^{-1} = 2300 (h^{-1}\text{Mpc})^3$.⁹ We also use this value to build up the analytical Gaussian covariance for both the power spectrum and bispectrum.

As a first step, we fit the PT challenge data taken from a single snapshot at z_3 ($z_{\text{eff}} = 0.61$) with the different analysis pipelines. We perform the analysis using the Gaussian covariance which corresponds to the cumulative volume of the BOSS survey, $5.8 (h^{-1}\text{Gpc})^3$, and to the total simulation volume, $566 (h^{-1}\text{Gpc})^3$.

Our results in the WC and EC3 models are shown in Fig. 1. The 1d marginalized constraints on cosmological and bias parameters are given in Tab. I.

Let us first discuss the analysis with the full simulation volume. We observe that the WC and EC3 pipelines yield significantly different posteriors. In particular, one can notice a significant, 5% bias in the recovery of σ_8 when the WC model is used. In the EC3 model, the systematic error associated with σ_8 is significantly smaller, being around 1%. The measurement of ω_{cdm} in the WC model shows a bias of 1.5%, whereas, in the EC3 pipeline, this shift is reduced to 0.5%. The recovery of h is unbiased in both WC and EC3 models, even when considering the total simulation volume. The second important observation is that the recovery of nuisance parameters is also biased when using the WC model.¹⁰ Namely, b_2 is lower than ground truth by ~ 1 , and b_1 is shifted toward lower values, a shift correlated with the bias in σ_8 . The EC3 pipeline demonstrates much better agreement with all values of bias parameters estimated in previous bispectrum analyses [28, 65, 66].

In the analysis with a covariance matrix rescaled to match the cumulative volume of the BOSS survey, we again observe significant differences in the posteriors between the WC and EC3 models. Specifically, in the WC model, ω_{cdm} and σ_8 deviate from their true values by σ_{BOSS} and $1.2\sigma_{\text{BOSS}}$, respectively, in terms of the statistical error from the analysis with the BOSS volume.

⁹ The mean galaxy densities are slightly different at z_1 and z_3 , but this difference is insignificant for the purposes of our analysis.

¹⁰ We consider estimates of nuisance parameters from the galaxy-matter cross power spectrum and the real space bispectrum [65, 66] as their “ground truth” values.

Notably, the mean value of ω_{cdm} is lower compared to the results from the full simulation volume. As we will demonstrate later, this shift arises from the fact that the WC model enforces $c_{e, \text{mono}} = 0$, and this bias is fully corrected after including a scale-dependent stochastic counterterm in the monopole. The bias in σ_8 recovery is entirely driven by the theory systematic error on this parameter. No prior volume effect on σ_8 is observed for the WC model. The situation is quite different for the EC3 model, where the shifts in cosmological parameters do not exceed $0.3\sigma_{\text{BOSS}}$. Interestingly, the projection effects for σ_8 work in the opposite direction, reducing the small systematic bias present in the $V = 566$ case. Unlike the WC model, the EC3 priors have a negligible impact on ω_{cdm} due to its consistent treatment of stochastic biases.

The recovery of nuisance parameters remains biased for the WC model, even for the errorbars corresponding to the volume of the BOSS survey. In particular, the $b_{\mathcal{G}_2} - b_2$ contour is shifted away from the ground truth by 2σ . These large shifts are related to the shifts in ω_{cdm} and σ_8 (for the WC model) and could be especially problematic for the analyses of non-local primordial non-Gaussianity (PNG), which is correlated with $b_{\mathcal{G}_2}$ and b_2 [42]. In contrast, the EC3 model allows for the recovery of all bias parameters within $\lesssim 0.5\sigma_{\text{BOSS}}$. In fact, the PNG analyses based on the CLASS-PT code [42, 43] used a somewhat lower power spectrum scale cut $k_{\text{max}} = 0.17 h\text{Mpc}^{-1}$, which completely eliminates the bias on the EFT parameters, c.f. [66].

The magnitude of projection effects increases with the number of nuisance parameters, leading the single-chunk analysis to somewhat underestimate the parameter shifts due to marginalization effects. To reliably assess the prior volume effects, we perform a multi-chunk analysis of four simulation samples – two at the z_1 redshift bin ($z_{\text{eff}} = 0.38$) and two at the z_3 redshift bin ($z_{\text{eff}} = 0.61$). For each data chunk, we introduce an independent set of EFT parameters, allowing them to vary freely in the analysis. The mock catalogues at the same redshift slice are designed to be identical emulating the BOSS samples in the Northern and Southern galactic caps (NGC and SGC). We adjust the volume for each chunk to match the actual BOSS volumes of the NGCz1, SGCz1, NGCz3, and SGCz3 caps, while keeping the PT Challenge mean galaxy density \bar{n}_{PTC} to allow for meaningful comparisons with previous results. We call this analysis $4 \times V = 5.8$.

The results of the multi-chunk analysis for the different

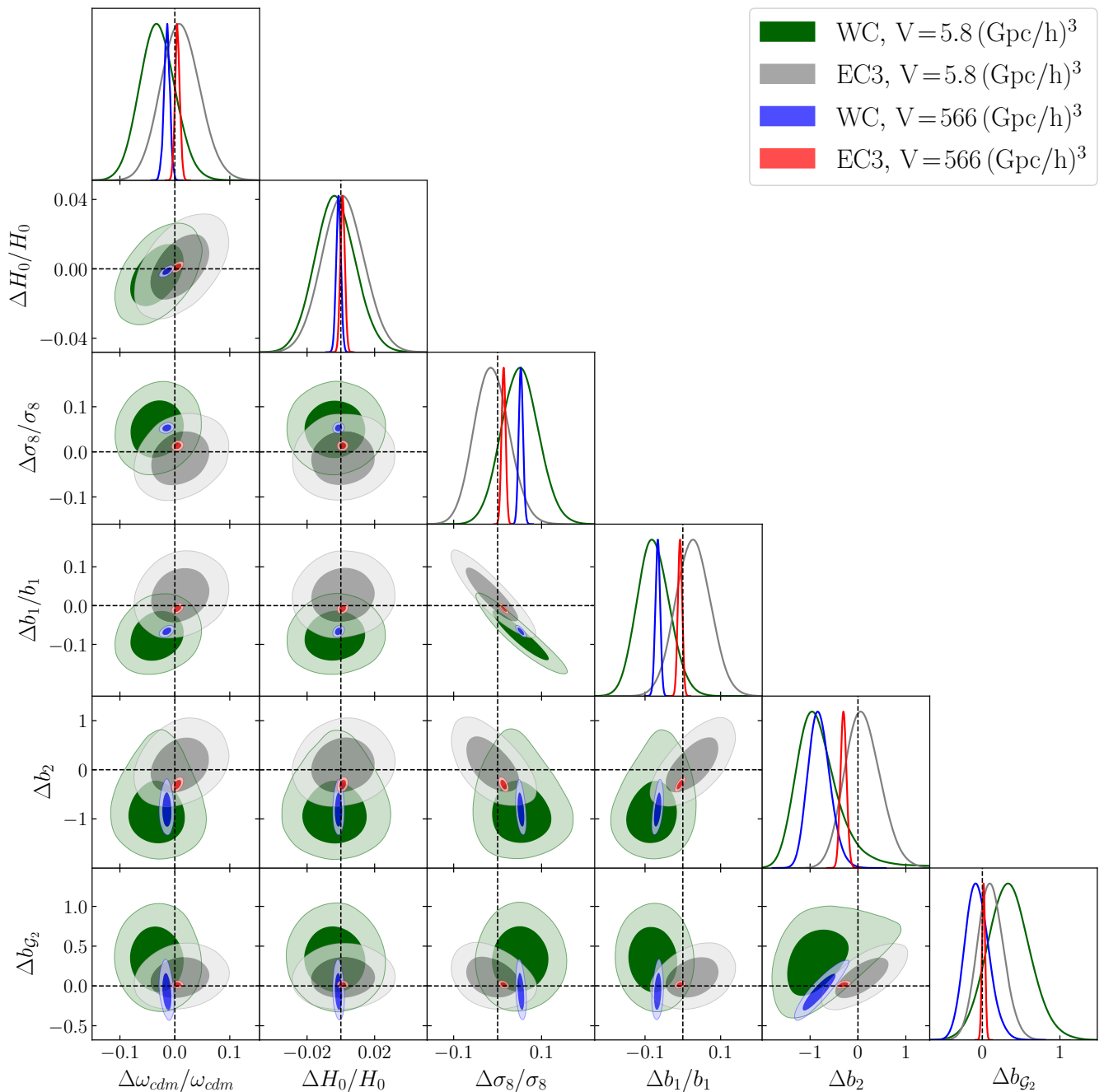


FIG. 1. Posterior distributions inferred from the single snapshot of the PT challenge simulation at $z_{\text{eff}} = 0.61$ in the WC and EC3 models using the analytical covariance matching the BOSS survey volume $5.8 (h^{-1}\text{Gpc})^3$, and the covariance corresponding to the total simulation volume $566 (h^{-1}\text{Gpc})^3$.

models are presented in Fig. 2. The corresponding 1d marginalized parameter constraints are given in Tab. I.

Let us quantify the projection effects for each model. We assess the amplitude of projection effects by calculating the difference in the parameter means between the $4 \times V$ and $V = 566$ analyses, and expressing the result

in units of the standard deviation from the $4 \times V$ analysis.¹¹ Starting with the WC model, we observe that the mean of ω_{cdm} in the multi-chunk analysis is shifted lower

¹¹ In the $V = 566$ analysis, the difference between the mean and best-fit values of parameters is negligible.

Model \ Param.	WC			EC1		
	$4 \times V = 5.8$	$V = 5.8$	$V = 566$	$4 \times V = 5.8$	$V = 5.8$	$V = 566$
$\Delta\omega_{cdm}/\omega_{cdm}$	$-0.038^{+0.030}_{-0.033}$	$-0.031^{+0.032}_{-0.034}$	$-0.015^{+0.0058}_{-0.0052}$	$-0.028^{+0.031}_{-0.035}$	$-0.015^{+0.034}_{-0.037}$	$-0.011^{+0.0045}_{-0.0050}$
$\Delta h/h$	$-0.004^{+0.012}_{-0.012}$	$-0.003^{+0.012}_{-0.013}$	$-0.0014^{+0.0015}_{-0.0014}$	$-0.002^{+0.012}_{-0.013}$	$-0.001^{+0.012}_{-0.013}$	$-0.0032^{+0.0014}_{-0.0014}$
$\Delta\sigma_8/\sigma_8$	$0.029^{+0.040}_{-0.042}$	$0.051^{+0.041}_{-0.044}$	$0.053^{+0.0049}_{-0.0051}$	$0.027^{+0.040}_{-0.043}$	$0.058^{+0.041}_{-0.044}$	$0.062^{+0.0045}_{-0.0046}$
$\Delta b_1/b_1$	–	$-0.077^{+0.041}_{-0.046}$	$-0.066^{+0.0065}_{-0.0062}$	–	$-0.069^{+0.042}_{-0.046}$	$-0.078^{+0.0050}_{-0.0049}$
Δb_2	–	$-0.77^{+0.31}_{-0.61}$	$-0.80^{+0.21}_{-0.25}$	–	$-0.38^{+0.37}_{-0.62}$	$-0.31^{+0.17}_{-0.18}$
$\Delta b_{\mathcal{G}_2}$	–	$0.34^{+0.27}_{-0.29}$	$-0.07^{+0.15}_{-0.17}$	–	$0.49^{+0.27}_{-0.28}$	$0.92^{+0.14}_{-0.14}$

Model \ Param.	EC2			EC2	EC3		
	$4 \times V = 5.8$	$V = 5.8$	$V = 566$	$k_{\max} = 0.2$ $V = 566$	$4 \times V = 5.8$	$V = 5.8$	$V = 566$
$\Delta\omega_{cdm}/\omega_{cdm}$	$-0.001^{+0.039}_{-0.042}$	$-0.006^{+0.044}_{-0.048}$	$-0.0085^{+0.0064}_{-0.0070}$	$-0.0066^{+0.0076}_{-0.0078}$	$0.002^{+0.031}_{-0.034}$	$0.010^{+0.035}_{-0.037}$	$0.0048^{+0.0043}_{-0.0046}$
$\Delta h/h$	$0.001^{+0.013}_{-0.013}$	$0.0^{+0.013}_{-0.014}$	$0.0002^{+0.0017}_{-0.0017}$	$-0.0034^{+0.0019}_{-0.0019}$	$0.001^{+0.012}_{-0.013}$	$0.001^{+0.012}_{-0.013}$	$0.0010^{+0.0013}_{-0.0013}$
$\Delta\sigma_8/\sigma_8$	$-0.018^{+0.042}_{-0.046}$	$0.037^{+0.044}_{-0.047}$	$0.051^{+0.0051}_{-0.0053}$	$0.026^{+0.0057}_{-0.0060}$	$-0.053^{+0.031}_{-0.035}$	$-0.013^{+0.039}_{-0.042}$	$0.014^{+0.0047}_{-0.0048}$
$\Delta b_1/b_1$	–	$-0.044^{+0.049}_{-0.051}$	$-0.057^{+0.0086}_{-0.0089}$	$-0.038^{+0.0091}_{-0.0087}$	–	$0.027^{+0.046}_{-0.048}$	$-0.0075^{+0.0057}_{-0.0059}$
Δb_2	–	$-0.33^{+0.66}_{-0.80}$	$-0.81^{+0.29}_{-0.31}$	$-0.62^{+0.36}_{-0.43}$	–	$0.11^{+0.35}_{-0.41}$	$-0.30^{+0.064}_{-0.066}$
$\Delta b_{\mathcal{G}_2}$	–	$0.25^{+0.37}_{-0.37}$	$-0.29^{+0.26}_{-0.26}$	$0.43^{+0.32}_{-0.32}$	–	$0.11^{+0.17}_{-0.18}$	$0.016^{+0.020}_{-0.021}$

TABLE I. Marginalized 1d constraints on the cosmological and bias parameters inferred from the single- and multi-chunk analyses of the PT Challenge simulation data for different models. The cosmological parameters are shown as $(p - p_{\text{fid}})/p_{\text{fid}}$, where p_{fid} denotes the fiducial value used in the simulation. For single-chunk analyses we also report constraints on the bias parameters. All volumes are expressed in units of $[h^{-1}\text{Gpc}]^3$.

compared to the $V = 566$ case. However, this shift does not scale with the number of boxes (or equivalently, with the number of nuisance parameters), therefore it cannot be explained by the usual marginalization effects caused by non-Gaussian correlations in the posteriors. Additionally, we identify a 0.6σ downward shift in σ_8 due to projection effects. Unlike the WC model, the EC1 setup shows unbiased recovery of ω_{cdm} in the $V = 5.8$ analysis. This suggests that adding a scale-dependent stochastic counterterm in the monopole is essential for unbiased inference of cosmological parameters. At the same time, allowing more flexibility in the stochasticity model slightly increases the Bayesian marginalization shift in ω_{cdm} and σ_8 to 0.5σ and 0.8σ , respectively.

The EC2 models shows a 1.6σ shift in σ_8 due to projection effects. Notably, the actual theory systematic bias in the recovery of σ_8 persists at the same 5% level observed in the WC model, indicating that this shift cannot be explained by the choice of priors. To elucidate the source

of this bias, we perform an additional analysis using EC2 priors but with $k_{\max} = 0.2 h\text{Mpc}^{-1}$ for both z_1/z_3 redshift bins, similar to the EC3 setup. This reduces the systematic bias in σ_8 by half, bringing it down to 2.6%. Thus, the bias on σ_8 is largely driven by the overoptimistic scale cuts in the WC model. In the EC3 model, we detect the projection effects for σ_8 at the 2.2σ level, while the other parameters remain unaffected. However, the mean of σ_8 is shifted by only 1.7σ from the ground truth, an acceptable shift in a typical Bayesian analysis. Importantly, the theory-driven systematic error on σ_8 is reduced to 1.4%, compared to 2.6% in the EC2 $k_{\max} = 0.2$ analysis. This improvement is attributed to the inclusion of bispectrum data, which breaks the degeneracies present at the power spectrum level and pulls the parameters closer to their true values.

All in all, we conclude that the WC model is somewhat restrictive. First, the posterior of ω_{cdm} is affected by the priors generated by the inaccuracy of the WC stochas-

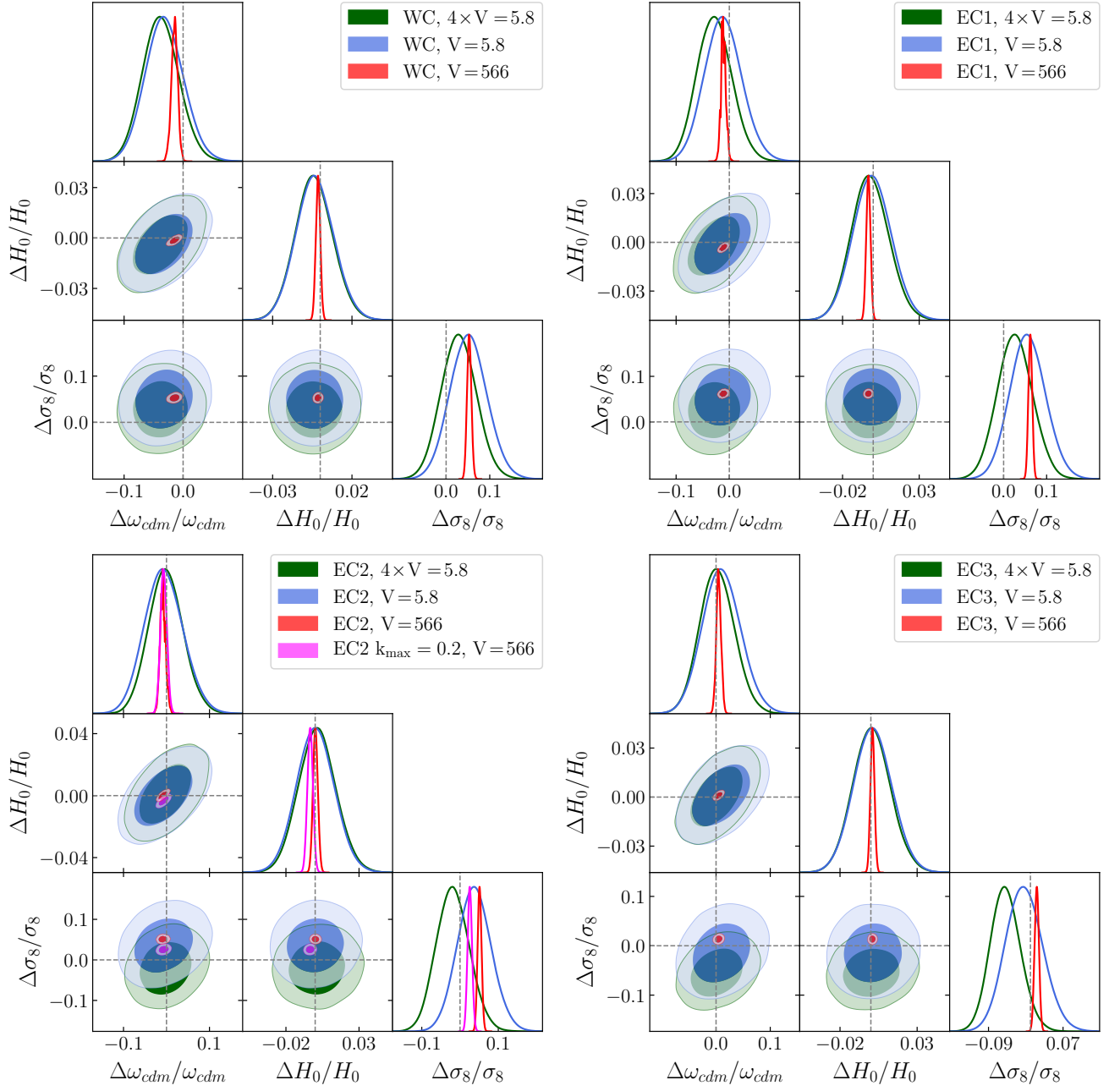


FIG. 2. Posterior distributions from the different analyses of the PT challenge simulation for the WC model (*upper left panel*), the EC1 model (*upper right panel*), the EC2 model (*lower left panel*) and the EC3 model (*lower right panel*). The results are inferred from the four BOSS-like data chunks (green), as well as from the single snapshot at $z_{\text{eff}} = 0.61$ with the covariance matching the BOSS survey volume (blue), and the covariance rescaled to match the full PT challenge volume $566 (h^{-1}\text{Gpc})^3$ (red). For the EC2 model, we also show the analysis with $k_{\text{max}} = 0.2 h\text{Mpc}^{-1}$ and the covariance corresponding to the full simulation volume (in pink).

ticity model. Second, the WC model applies overoptimistic scale cuts in the z_3 redshift bin which significantly bias parameter recovery, overestimating σ_8 by more than 5%. Unlike the Bayesian marginalization effect, this is a genuine systematic bias that does not vanish with bet-

ter priors or larger data volumes. In contrast, the EC3 model leads to a small ($< 1.5\%$) systematic bias in the recovery of cosmological parameters. This bias constitutes a small negligible fraction of the statistical error in the actual BOSS data. Using more observables, like the

cross-correlation with CMB lensing or imposing informative simulation-based priors on nuisance parameters from [18] can mitigate the Bayesian marginalization effects present in the EC3 analysis with the BOSS volume.

4.2. BOSS-like analysis

Here, we explore the implications of Bayesian marginalization effects and theory systematic bias within a realistic analysis framework. To that end, we perform a multi-chunk analysis of the four simulation samples using the actual BOSS data covariance estimated from the Patchy mocks. This allows us to closely reproduce the actual BOSS data analysis. Additionally, to evaluate the systematic error, we perform a separate analysis using Gaussian covariance corresponding to 100 times the actual volume of each BOSS-like data chunk, yielding a cumulative volume of $580 (h^{-1}\text{Gpc})^3$. For this analysis, we adopt the actual galaxy number density of the PT Challenge simulation to reduce the impact of marginalization projection effects. Note that we do not utilize the empirical covariance from the Patchy mocks in the $100 \times V_{\text{BOSS}}$ analysis due to sample noise, which is particularly significant for bispectrum measurements. We refer to these analyses as V_{BOSS} and $100 \times V_{\text{BOSS}}$, respectively.

Our results are shown in Fig. 3. The marginalized parameter constraints are listed in Tab. II. In the WC model, we observe a 0.8σ shift in ω_{cdm} from the ground truth for the covariance of the V_{BOSS} volume, caused by the inaccuracy of the WC template. We identify a 5% systematic error on σ_8 from the $100 \times V_{\text{BOSS}}$ analysis, in perfect agreement with the results from the PT Challenge analysis. In contrast, the EC2 model provides an unbiased measurement of ω_{cdm} due to the consistent treatment of stochastic bias. The EC3 model leads to a small systematic bias in the recovery of cosmological parameters, with the largest 1.5% error on σ_8 . However, the broader priors in EC3 induce a somewhat larger marginalization projection shift of about 2σ for σ_8 . This shift is generally acceptable in a Bayesian analysis. It can be reduced by imposing correlated priors on the EFT parameters, as discussed in [67]. An alternative and more motivated from the Bayesian point of view approach is to employ simulation-based priors from [18].

Let us comment on the large bias that we have seen in the WC model. A natural question is why this has not

been identified before in the analyses of [2, 67]? These studies mostly focused on the Nseries simulations whose volume is smaller than PT Challenge and which implements the effects of the survey selection function and survey geometry. The Nseries mocks were also analyzed in detail with the pipeline associated with the CLASS-PT code in [5, 22, 28]. These papers found an excellent agreement between analyses based on PT Challenge and Nseries, which served as a validation of the window-free method of [68, 69] used in these works. The only difference w.r.t. the studies based on the PyBird code is that they used the standard forward model for the survey geometry, as opposed to the window-free method. This suggests that the apparent tension between the Nseries analyses of WC and EC might stem from inaccuracies in the window function treatment used by the WC team.

Let us compare now our results with the relatively recent analysis of projection effects performed in [24]. The key difference with our approach is that their analysis uses synthetic data generated from the best-fit model to BOSS data. [24] report a downward shift in the mean value of σ_8 at the 1.2σ level for the WC model and at the 1.8σ level for the EC model. Our results, presented in Tab. II, show similar marginalization shifts: 1.4σ for the WC model and 2.2σ for the EC3 model.¹² Given the differences in our analysis methodologies (e.g., Ref. [24] does not use bispectrum measurements), this is a good agreement. The virtue of the present analysis is that it is based on simulation data, allowing us to directly estimate the theory-driven systematic bias in parameter recovery.

Let us also point out that Ref. [24] did not include the bispectrum and did not consistently use the $k_{\text{max}} = 0.2 h\text{Mpc}^{-1}$ in their reproduction of the analysis pipeline based on the CLASS-PT code. Both of these choices lead to a larger best-fit value of σ_8 , which agrees with the WC results, but is actually biased higher than the true value by $\approx 5\%$. The comparison of EC and WC analysis choices in these inconsistent settings may lead to misleading conclusions. This issue is particularly important in the con-

¹² Ref. [24] estimates the projections effects by calculating the parameter differences w.r.t. the best-fit prediction. To provide a meaningful comparison with their results, we compute the marginalization shift here as the difference in parameter means between the V_{BOSS} and $100 \times V_{\text{BOSS}}$ analyses. We have checked that for $100 \times V_{\text{BOSS}}$ the difference between the mean and best-fit values of parameters is negligible.

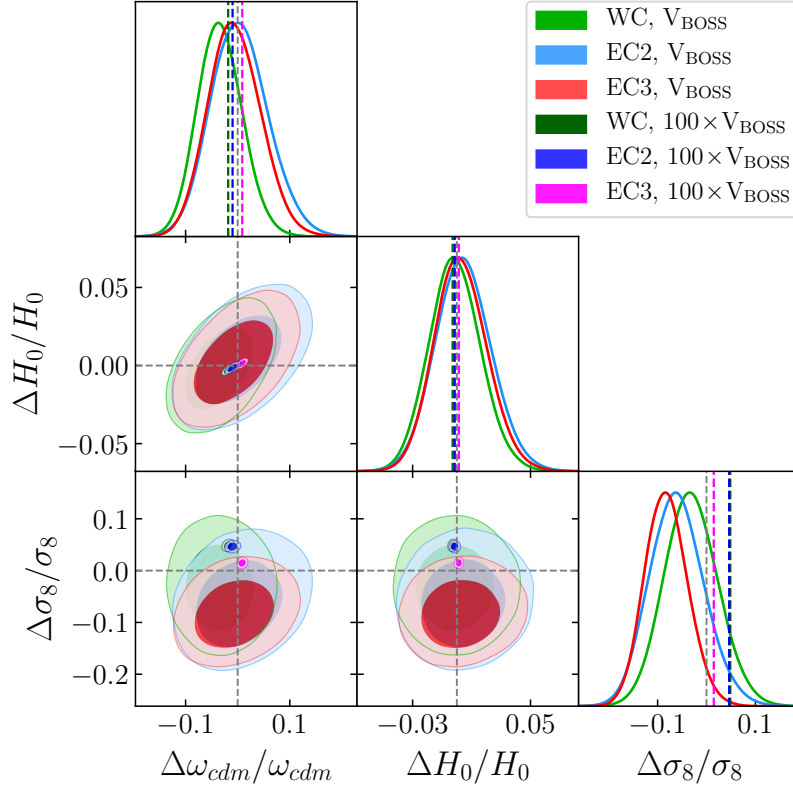


FIG. 3. Posterior distributions inferred from the four BOSS-like samples of the PT Challenge simulation using the BOSS data covariance estimated from the Patchy mocks (V_{BOSS}) and the analytical Gaussian covariance corresponding to 100 times the BOSS volume ($100 \times V_{\text{BOSS}}$). For $100 \times V_{\text{BOSS}}$, only the mean values of the corresponding parameters are depicted by dashed lines.

Model \ Param.	WC		EC2		EC3	
	V_{BOSS}	$100 \times V_{\text{BOSS}}$	V_{BOSS}	$100 \times V_{\text{BOSS}}$	V_{BOSS}	$100 \times V_{\text{BOSS}}$
$\Delta\omega_{\text{cdm}}/\omega_{\text{cdm}}$	$-0.034^{+0.041}_{-0.047}$	$-0.018^{+0.005}_{-0.005}$	$0.004^{+0.052}_{-0.060}$	$-0.0098^{+0.0061}_{-0.0065}$	$-0.006^{+0.048}_{-0.054}$	$0.0088^{+0.0043}_{-0.0047}$
$\Delta h/h$	$-0.001^{+0.017}_{-0.018}$	$-0.0028^{+0.0014}_{-0.0014}$	$0.004^{+0.019}_{-0.020}$	$-0.0015^{+0.0016}_{-0.0017}$	$0.003^{+0.017}_{-0.019}$	$0.0014^{+0.0014}_{-0.0014}$
$\Delta\sigma_8/\sigma_8$	$-0.031^{+0.054}_{-0.058}$	$0.049^{+0.005}_{-0.005}$	$-0.060^{+0.053}_{-0.061}$	$0.046^{+0.005}_{-0.005}$	$-0.082^{+0.041}_{-0.047}$	$0.015^{+0.005}_{-0.005}$

TABLE II. Marginalized 1d constraints on the cosmological parameters from the BOSS-like analyses of the four simulation samples for three models and two choices of the covariance matrix. All parameters are shown as $(p - p_{\text{fid}})/p_{\text{fid}}$, where p_{fid} represents the fiducial value used in the simulations.

text of profile likelihood analysis, where a recent study of early dark energy [70] used $k_{\text{max}} = 0.25 h \text{Mpc}^{-1}$, which, as we show here, introduces a significant bias in the σ_8 recovery.

Acknowledgments. MI thanks George Efstathiou for inspiring discussions. We thank Guido D’Amico for

encouraging us to publish this note. All numerical calculations have been performed with the Helios cluster at the Institute for Advanced Study, Princeton. This work was supported in part by MEXT/JSPS KAKENHI Grant Numbers JP20H05861, JP21H01081, JP22K03634, JP24H00215 and JP24H00221.

[1] M. M. Ivanov, M. Simonović, and M. Zaldarriaga, *JCAP* **05**, 042 (2020), arXiv:1909.05277 [astro-ph.CO].

[2] G. D’Amico, J. Gleyzes, N. Kokron, D. Markovic, L. Sen-

- atore, P. Zhang, F. Beutler, and H. Gil-Marín, (2019), [arXiv:1909.05271 \[astro-ph.CO\]](#).
- [3] O. H. E. Philcox, M. M. Ivanov, M. Simonović, and M. Zaldarriaga, *JCAP* **05**, 032 (2020), [arXiv:2002.04035 \[astro-ph.CO\]](#).
- [4] S.-F. Chen, Z. Vlah, and M. White, *JCAP* **02**, 008 (2022), [arXiv:2110.05530 \[astro-ph.CO\]](#).
- [5] O. H. E. Philcox and M. M. Ivanov, *Phys. Rev. D* **105**, 043517 (2022), [arXiv:2112.04515 \[astro-ph.CO\]](#).
- [6] A. Chudaykin and M. M. Ivanov, *Phys. Rev. D* **107**, 043518 (2023), [arXiv:2210.17044 \[astro-ph.CO\]](#).
- [7] D. Baumann, A. Nicolis, L. Senatore, and M. Zaldarriaga, *JCAP* **1207**, 051 (2012), [arXiv:1004.2488 \[astro-ph.CO\]](#).
- [8] J. J. M. Carrasco, M. P. Hertzberg, and L. Senatore, *JHEP* **09**, 082 (2012), [arXiv:1206.2926 \[astro-ph.CO\]](#).
- [9] M. M. Ivanov, “Effective Field Theory for Large-Scale Structure,” (2023) [arXiv:2212.08488 \[astro-ph.CO\]](#).
- [10] D. Blas, M. Garny, M. M. Ivanov, and S. Sibiryakov, *JCAP* **1607**, 052 (2016), [arXiv:1512.05807 \[astro-ph.CO\]](#).
- [11] D. Blas, M. Garny, M. M. Ivanov, and S. Sibiryakov, *JCAP* **1607**, 028 (2016), [arXiv:1605.02149 \[astro-ph.CO\]](#).
- [12] S.-F. Chen, Z. Vlah, and M. White, *JCAP* **07**, 062 (2020), [arXiv:2005.00523 \[astro-ph.CO\]](#).
- [13] S.-F. Chen, Z. Vlah, E. Castorina, and M. White, *JCAP* **03**, 100 (2021), [arXiv:2012.04636 \[astro-ph.CO\]](#).
- [14] D. Wadekar, M. M. Ivanov, and R. Scoccimarro, *Phys. Rev. D* **102**, 123521 (2020), [arXiv:2009.00622 \[astro-ph.CO\]](#).
- [15] G. Cabass, M. M. Ivanov, O. H. E. Philcox, M. Simonovic, and M. Zaldarriaga, *Phys. Lett. B* **841**, 137912 (2023), [arXiv:2211.14899 \[astro-ph.CO\]](#).
- [16] M. M. Ivanov, C. Cuesta-Lazaro, S. Mishra-Sharma, A. Obuljen, and M. W. Toomey, *Phys. Rev. D* **110**, 063538 (2024), [arXiv:2402.13310 \[astro-ph.CO\]](#).
- [17] G. Cabass, O. H. E. Philcox, M. M. Ivanov, K. Akitsu, S.-F. Chen, M. Simonović, and M. Zaldarriaga, (2024), [arXiv:2404.01894 \[astro-ph.CO\]](#).
- [18] M. M. Ivanov, A. Obuljen, C. Cuesta-Lazaro, and M. W. Toomey, (2024), [arXiv:2409.10609 \[astro-ph.CO\]](#).
- [19] R. O’Shaughnessy, B. Farr, E. Ochsner, H.-S. Cho, C. Kim, and C.-H. Lee, *Phys. Rev. D* **89**, 064048 (2014), [arXiv:1308.4704 \[gr-qc\]](#).
- [20] S. Biscoveanu, C. Talbot, and S. Vitale, *Mon. Not. Roy. Astron. Soc.* **511**, 4350 (2022), [arXiv:2111.13619 \[astro-ph.HE\]](#).
- [21] S. Olsen, J. Roulet, H. S. Chia, L. Dai, T. Venumadhav, B. Zackay, and M. Zaldarriaga, *Phys. Rev. D* **104**, 083036 (2021), [arXiv:2106.13821 \[astro-ph.HE\]](#).
- [22] A. Chudaykin, K. Dolgikh, and M. M. Ivanov, *Phys. Rev. D* **103**, 023507 (2021), [arXiv:2009.10106 \[astro-ph.CO\]](#).
- [23] A. Chudaykin, M. M. Ivanov, O. H. E. Philcox, and M. Simonović, *Phys. Rev. D* **102**, 063533 (2020), [arXiv:2004.10607 \[astro-ph.CO\]](#).
- [24] T. Simon, P. Zhang, V. Poulin, and T. L. Smith, *Phys. Rev. D* **107**, 123530 (2023), [arXiv:2208.05929 \[astro-ph.CO\]](#).
- [25] S. Alam *et al.* (BOSS), *Mon. Not. Roy. Astron. Soc.* **470**, 2617 (2017), [arXiv:1607.03155 \[astro-ph.CO\]](#).
- [26] R. Laureijs *et al.* (EUCLID), (2011), [arXiv:1110.3193 \[astro-ph.CO\]](#).
- [27] A. Aghamousa *et al.* (DESI), (2016), [arXiv:1611.00036 \[astro-ph.IM\]](#).
- [28] M. M. Ivanov, O. H. E. Philcox, G. Cabass, T. Nishimichi, M. Simonović, and M. Zaldarriaga, *Phys. Rev. D* **107**, 083515 (2023), [arXiv:2302.04414 \[astro-ph.CO\]](#).
- [29] S.-F. Chen, M. M. Ivanov, O. H. E. Philcox, and L. Wenzl, (2024), [arXiv:2406.13388 \[astro-ph.CO\]](#).
- [30] K. Akitsu, (2024), [arXiv:2410.08998 \[astro-ph.CO\]](#).
- [31] J. M. Sullivan, U. Seljak, and S. Singh, *JCAP* **11**, 026 (2021), [arXiv:2104.10676 \[astro-ph.CO\]](#).
- [32] T. Baldauf, M. Mirbabayi, M. Simonović, and M. Zaldarriaga, (2016), [arXiv:1602.00674 \[astro-ph.CO\]](#).
- [33] A. Chudaykin, M. M. Ivanov, and M. Simonović, *Phys. Rev. D* **103**, 043525 (2021), [arXiv:2009.10724 \[astro-ph.CO\]](#).
- [34] T. Nishimichi, G. D’Amico, M. M. Ivanov, L. Senatore, M. Simonović, M. Takada, M. Zaldarriaga, and P. Zhang, *Phys. Rev. D* **102**, 123541 (2020), [arXiv:2003.08277 \[astro-ph.CO\]](#).
- [35] E. Krause *et al.* (Beyond-2pt), (2024), [arXiv:2405.02252 \[astro-ph.CO\]](#).
- [36] G. D’Amico, L. Senatore, and P. Zhang, *JCAP* **01**, 006 (2021), [arXiv:2003.07956 \[astro-ph.CO\]](#).
- [37] J. Hartlap, P. Simon, and P. Schneider, *Astron. Astrophys.* **464**, 399 (2007), [arXiv:astro-ph/0608064](#).
- [38] E. Sellentin and A. F. Heavens, *Mon. Not. Roy. Astron. Soc.* **456**, L132 (2016), [arXiv:1511.05969 \[astro-ph.CO\]](#).
- [39] C. Howlett and W. J. Percival, *Mon. Not. Roy. Astron. Soc.* **472**, 4935 (2017), [arXiv:1709.03057 \[astro-ph.CO\]](#).
- [40] O. H. E. Philcox, M. M. Ivanov, M. Zaldarriaga, M. Simonovic, and M. Schmittfull, *Phys. Rev. D* **103**, 043508 (2021), [arXiv:2009.03311 \[astro-ph.CO\]](#).
- [41] F.-S. Kitaura *et al.*, *Mon. Not. Roy. Astron. Soc.* **456**, 4156 (2016), [arXiv:1509.06400 \[astro-ph.CO\]](#).
- [42] G. Cabass, M. M. Ivanov, O. H. E. Philcox, M. Simonović, and M. Zaldarriaga, *Phys. Rev. Lett.* **129**, 021301 (2022), [arXiv:2201.07238 \[astro-ph.CO\]](#).
- [43] G. Cabass, M. M. Ivanov, O. H. E. Philcox, M. Si-

- monović, and M. Zaldarriaga, *Phys. Rev. D* **106**, 043506 (2022), [arXiv:2204.01781 \[astro-ph.CO\]](#).
- [44] G. D’Amico, M. Lewandowski, L. Senatore, and P. Zhang, (2022), [arXiv:2201.11518 \[astro-ph.CO\]](#).
- [45] M. M. Ivanov, M. Simonović, and M. Zaldarriaga, *Phys. Rev. D* **101**, 083504 (2020), [arXiv:1912.08208 \[astro-ph.CO\]](#).
- [46] M. M. Ivanov, E. McDonough, J. C. Hill, M. Simonović, M. W. Toomey, S. Alexander, and M. Zaldarriaga, *Phys. Rev. D* **102**, 103502 (2020), [arXiv:2006.11235 \[astro-ph.CO\]](#).
- [47] W. L. Xu, J. B. Muñoz, and C. Dvorkin, *Phys. Rev. D* **105**, 095029 (2022), [arXiv:2107.09664 \[astro-ph.CO\]](#).
- [48] R. C. Nunes, S. Vagnozzi, S. Kumar, E. Di Valentino, and O. Mena, *Phys. Rev. D* **105**, 123506 (2022), [arXiv:2203.08093 \[astro-ph.CO\]](#).
- [49] S. Kumar, R. C. Nunes, and P. Yadav, *JCAP* **09**, 060 (2022), [arXiv:2205.04292 \[astro-ph.CO\]](#).
- [50] H. Rubira, A. Mazoun, and M. Garny, *JCAP* **01**, 034 (2023), [arXiv:2209.03974 \[astro-ph.CO\]](#).
- [51] K. K. Rogers, R. Hložek, A. Laguë, M. M. Ivanov, O. H. E. Philcox, G. Cabass, K. Akitsu, and D. J. E. Marsh, *JCAP* **06**, 023 (2023), [arXiv:2301.08361 \[astro-ph.CO\]](#).
- [52] A. He, M. M. Ivanov, R. An, and V. Gluscevic, *Astrophys. J. Lett.* **954**, L8 (2023), [arXiv:2301.08260 \[astro-ph.CO\]](#).
- [53] A. He, R. An, M. M. Ivanov, and V. Gluscevic, *Phys. Rev. D* **109**, 103527 (2024), [arXiv:2309.03956 \[astro-ph.CO\]](#).
- [54] D. Camarena, F.-Y. Cyr-Racine, and J. Houghtling, *Phys. Rev. D* **108**, 103535 (2023), [arXiv:2309.03941 \[astro-ph.CO\]](#).
- [55] E. McDonough, J. C. Hill, M. M. Ivanov, A. La Posta, and M. W. Toomey, *Int. J. Mod. Phys. D* **33**, 2430003 (2024), [arXiv:2310.19899 \[astro-ph.CO\]](#).
- [56] A. Chudaykin and M. M. Ivanov, *JCAP* **11**, 034 (2019), [arXiv:1907.06666 \[astro-ph.CO\]](#).
- [57] L. Senatore, *JCAP* **1511**, 007 (2015), [arXiv:1406.7843 \[astro-ph.CO\]](#).
- [58] M. Mirbabayi, F. Schmidt, and M. Zaldarriaga, *JCAP* **1507**, 030 (2015), [arXiv:1412.5169 \[astro-ph.CO\]](#).
- [59] S. Alam *et al.* (BOSS), *Mon. Not. Roy. Astron. Soc.* **470**, 2617 (2017), [arXiv:1607.03155 \[astro-ph.CO\]](#).
- [60] M. Schmittfull, M. Simonović, V. Assassi, and M. Zaldarriaga, *Phys. Rev. D* **100**, 043514 (2019), [arXiv:1811.10640 \[astro-ph.CO\]](#).
- [61] M. Schmittfull, M. Simonović, M. M. Ivanov, O. H. E. Philcox, and M. Zaldarriaga, (2020), [arXiv:2012.03334 \[astro-ph.CO\]](#).
- [62] P. Taule and M. Garny, *JCAP* **11**, 078 (2023), [arXiv:2308.07379 \[astro-ph.CO\]](#).
- [63] T. Colas, G. D’Amico, L. Senatore, P. Zhang, and F. Beutler, *JCAP* **06**, 001 (2020), [arXiv:1909.07951 \[astro-ph.CO\]](#).
- [64] M. M. Ivanov, O. H. E. Philcox, M. Simonović, M. Zaldarriaga, T. Nishimichi, and M. Takada, (2021), [arXiv:2110.00006 \[astro-ph.CO\]](#).
- [65] M. M. Ivanov, O. H. E. Philcox, T. Nishimichi, M. Simonović, M. Takada, and M. Zaldarriaga, *Phys. Rev. D* **105**, 063512 (2022), [arXiv:2110.10161 \[astro-ph.CO\]](#).
- [66] O. H. E. Philcox, M. M. Ivanov, G. Cabass, M. Simonović, M. Zaldarriaga, and T. Nishimichi, *Phys. Rev. D* **106**, 043530 (2022), [arXiv:2206.02800 \[astro-ph.CO\]](#).
- [67] G. D’Amico, Y. Donath, M. Lewandowski, L. Senatore, and P. Zhang, *JCAP* **05**, 059 (2024), [arXiv:2206.08327 \[astro-ph.CO\]](#).
- [68] O. H. E. Philcox, *Phys. Rev. D* **103**, 103504 (2021), [arXiv:2012.09389 \[astro-ph.CO\]](#).
- [69] O. H. E. Philcox, (2021), [arXiv:2107.06287 \[astro-ph.CO\]](#).
- [70] L. Herold and E. G. M. Ferreira, *Phys. Rev. D* **108**, 043513 (2023), [arXiv:2210.16296 \[astro-ph.CO\]](#).